Enhancing the performance of dye-sensitized solar cells by benzoic acid modified TiO_2 nanorod electrode

Jincheng Liu*, Yinjie Wang, Darren Sun*

School of Civil and Environmental Engineering, Nanyang Technological University, Singapore 639798. Fax: +65-67910676; Tel: +65-67906273
Corresponding authors: *JCLIU@ntu.edu.sg (J Liu); *DDSun@ntu.edu.sg (DD Sun)

ABSTRACT

The anatase TiO_2 nanorods capped by oleic acid with the length of 30-50 nm and diameter of approximately 4-5 nm were prepared by a facile two-phase hydrothermal method. The oleic acid ligands attached on the surface of TiO_2 nanorods were completely exchanged by benzoic acid ligands. The dye-sensitized solar cell (DSSC) fabricated based on the benzoic acid modified TiO_2 nanorod electrodes exhibited a higher power conversion efficiency of 6.37% than that (5.1%) of the P25 TiO_2 based DSSC. The surface modification by benzoic acid can effectively improve the hydrophility of TiO_2 nanorods, leading to an increased short circuit current density and a higher open circuit voltage. This study provided a facile alternative method to fabricate highly efficient TiO_2 nanorod-based electrodes for DSSCs.

Keywords*:* TiO_2; Nanorods; Ligand exchange; Dye-sensitized solar cells

1. Introduction

Due to its low cost, easy fabrication in the air, and high power conversion efficiency, dye-sensitized solar cells (DSSCs) have attracted wide research interests since 1991[1-3]. DSSCs are normally composed of porous dye-sensitized metal oxide photoanode, electrolyte, and counter electrode [4]. A porous nanocrystalline TiO_2 electrode coated with a dye sensitizer has been extensively used, and plays a key role in the light-harvesting and charge

diffusion in DSSCs. It is well known that the kinetics of electron diffusion in the TiO_2 porous layer is affected by trapping/detrapping events occurring along the sites of the electron traps such as defects, grain boundaries, and surface states [5, 6]. In order to improve the overall solar cell performance, it is essential to control the size and morphology of TiO_2 nanocrystals and optimize the nanostructure of its corresponding photoanode films.

One-dimensional nanocrystals have direct charge transfer path, which can effectively increase the charge transfer in the nonstructural photovoltaic cells [7-9]. Many earlier works reported the application of TiO_2 nanowire, TiO_2 nanofiber and TiO_2 nanorod (TiO_2 NR) in the photoanodes of DSSCs [10-15]. However, because of the large size of the one-dimensional TiO_2 nanocrystals, the properties of DSSCs were limited by the low extent of dye adsorption due to the relatively small specific surface area. In 2008, Kang et al. reported that the DSSC with the photoanode based on smaller TiO_2 NRs (4 nm $\times$ 20 nm sized) showed an increased charge transfer than the 6 nm sized nanoparticle-based films [16]. However, the control of size and morphology of TiO_2 NRs is not well with the Pluronic P-123 surfactant. Most recently, Lee et al. [17] and Marco et al. [18] prepared the small sizeTiO_2 NRs with better size and morphology control through a two-step hydrothermal method and the solvothermal approaches in benzyl alcohol, respectively. Accordingly, they got the increased power conversion efficiency (PCE) of 7.2% and 7.9%, respectively. It suggests that combining the merits of large surface area and efficient electron transfer can be possibly realized by the control of the size and morphology of the TiO_2 nanocrystals.

Oleic acid is widely used in the synthesis of TiO_2 NRs in the low-temperature hydrolysis and non-hydraulic sol-gel method by oriented attachment mechanisms [19-21]. Pyo et al.

reported the application of oleic acid capped TiO_2 NRs in the photoanode of DSSCs [22]. However, the efficiency is low even with the composition of nanoparticles and nanorods because oleic acid capped TiO_2 nanocrystals are hydrophobic, which lowers the uniformity of the TiO_2 NR paste. It is important to perform a ligand-exchange process before the application of oleic acid capped TiO_2 NRs in the DSSCs to make the material hydrophilic.

In the present study, anatase TiO_2 NRs with uniform morphology and size were synthesized by a facile two-phase sol-gel method. The synthesized oleic acid capped TiO_2 NRs were suffered a ligand exchange process by benzoic acid in order to get increased hydrophility. The TiO_2 NRs capped with different surfactants were used to make porous photoanodes of DSSCs. To the best of our knowledge, it is the first time to report using the hydrophobic oleic acid capped TiO_2 NRs in the photoanode of DSSCs after a ligand exchange process. We demonstrate that the ligand exchange process could enhance the properties of DSSC significantly by increasing the quality of the porous TiO_2 NR films. Small size TiO_2 NRs with large surface area and direct charge transfer path can increase the amount of adsorbed dye-sensitizers, facilitate the transfer of photo-generated carriers, and enhance the PCE of the DSSCs.

2. Experimental Section

2.1 Materials

Titanium tetraisopropoxide (TTIP, 97%), benzoic acid (BA,99%), oleic acid (OLA, technical, 90%), tert-butylamine (TBA, 99.5%), 4-tert-butylpyridine(99%), sodium iodide (NaI, 99%**),** iodine (I_2, 99 %), and polyoxyethylene (PEO, mw≈35,000) were purchased from Sigma-Aldrich Chemical Company. Acetyl acetone (AcAc, 99%) was purchased from

Alfa-Aesar. Dye N-719 was purchased from Solaronix Company. TiO_2 powder (P25) was purchase from Degussa Company. All solvents were of analytical grade and purchased from Sigma-Aldrich Company.

2.2 Synthesis and surface modification of TiO_2 NRs, and paste preparations

OLA capped anatase TiO_2 NRs were synthesized by a big modification of a reported two-phase hydrothermal process with the increasing of the TTIP concentration [23, 24]. Briefly, 0.9 mL of *tert*-butylamine was added to 10.0 mL of deionized water. At the same time, 0.9 mL of Titanium-*n*-propoxide was added into 18 mL of OLA. The above two solutions were then mixed and transferred to a Teflon-lined stainless steel autoclave. Hydrothermal synthesis was conducted at 180℃ for 6 h in an electric oven. After the reaction, the reacted mixtures were precipitated and washed with ethanol twice.

After the purified procedure was repeated for more than 6 times, the TiO_2 NRs was redispersed in tetrahydrofuran (THF) for the further ligand exchange process. A quantum of benzoic acid was then added into the solution of TiO_2 NRs in THF to make the concentration of benzoic acid to be 0.4 mol L^{-1}. The mixed solution was kept sonicating for 2 h, and then stirring for 24 h to exchange oleic acid completely. The as-prepared BA-capped TiO_2 NRs (BA-TiO_2) were then precipitated by adding excess ethanol, and centrifuged at 10000 rpm for the further preparation of TiO_2 paste.

To obtain the TiO_2 paste for doctor-blading process, 500 mg of TiO_2 (P25, OLA-TiO_2 NR, and BA-TiO_2 NR) and 167 mg of polyethylene oxide (mw≈35000) were added into the mixed solvents of 0.67 ml of deionized water and 0.17 mL of ethanol. The mixtures were then sonicated for 6 h to obtain homogeneous TiO_2 pastes for the fabrication of DSSCs.

2.3 Fabrication and test of dye-sensitized solar cells

Fluorine-doped tin oxide (FTO) conducting glasses were cleaned in a detergent solution using an ultrasonic bath for 15 min, then washed with DI water and ethanol. The TiO_2 paste was deposited onto the FTO glass by the doctor-blading process. Scotch tape with the thickness of 50 μm with a round hole of 0.28 cm^2 was employed to control the thickness and the active area of the film. The FTO glass samples coated with the TiO_2 pastes (P25, OLA-TiO_2 NRs, and BA-TiO_2 NRs) were then sintered at 450 ℃ for 30 min. After cooling to 70 ℃, the TiO_2 electrodes were immersed into a solution of 0.5 mmol L^{-1} (bis(tetrabutylammonium)- *cis*-di(thiocyanato)-*N*,*N*′-bis (4-carboxylato-4′-carboxylic acid-2,2-bipyridine) ruthenium(II) (N719) in a mixture of acetonitrile and *tert*-butyl alcohol (v/v, 1:1) and kept at room temperature for 24 h.

The solar cells were assembled by placing a platinum-sputered FTO (counter electrode) on the N719 dye-sensitized photoelectrode with hot-melt Surlyn film (50 μm thickness, Dupont) as a spacer. The sandwich type devices were assembled under a hot-press procedure for 5 minutes at 85 ℃. The redox electrolyte was introduced into the space of inter-electrodes through the siphon effect by dropping the electrolyte into the gap of the two electrodes. The gaps were sealed up by UV light-cure adhesives. The redox electrolyte used was 0.1 mol L^{-1} LiI, 0.05 mol L^{-1} I_2, 0.6 mol L^{-1} 1-methyl- 3-propylimidazolium iodide, and 0.5 mol L^{-1} *tert*-butylpyridine in dried acetonitrile [25].

2.4 Characterizations

Transmission electron microscopy (TEM) and high-resolution TEM (HRTEM) images were obtained using a JEOL 2010-H microscope operating at 200 kV. Fourier transform

infrared spectroscopy (FTIR) spectra were recorded in the range of 4000~400 cm^{-1} on a Perkin Elmer GX FT-IR system using compressed KBr disc technique. X-ray diffraction (XRD) patterns were taken on Bruker AXS D8 Advance using Cu Kα irradiation (λ=1.5406 Å). Scanning electron microscope (SEM) images were examined with ZEISS EVO 50 s electron microscopy.

The photocurrent-voltage (*J-V*) characteristics were measured with Keithley 2400 source meter. Power conversion efficiencies (PCE) were measured under an AM1.5 solar simulator. The UV-vis absorption spectra were recorded by using an Evolution 300 spectrophotometer. Before the UV test, the dye-sensitized TiO_2 porous electrodes on FTO were desorbed in 0.1 mol L^{-1} NaOH aqueous solution (2 mL) for 10 minutes. Electrochemical impedance spectroscopy (EIS) was performed on the DSSC devices under dark with the bias of 0.6 V by electrochemical station Autolab potentiostat 302.N and FRA2.

3. Results and discussions:

3.1 Characterizations of TiO_2 NRs.

Due to the fast reactivity of titanium alkoxides with water, it is difficult to control the morphology and size of TiO_2 nanocrystals [19]. With the addition of oleic acid, the TTIP precursor will react with oleic acid to form the titanium oleate complex with low hydrolysis activity, which can effectively fulfill the separation of nucleation and growth during the synthesis of TiO_2 nanocrystals. Moreover, the optional adherence of oleic acid to the aspects of TiO_2 nanocrystals can prevent the aggregation and control the directional growth of one-dimentional TiO_2 NRs. Here we use oleic acid as stabilizer in a two-phase hydrothermal method to prepare TiO_2 NRs for the first time.

As shown in Fig. 1a, the TiO_2 NRs synthesized using the hydrothermal method are typically anisotropic with 4-5 nm in diameter and 30-50 nm in length. The low- resolution TEM image reveals the TiO_2 NRs capped by OLA are well dispersed without evident aggregations (Fig. 1a), and the HRTEM image shows the TiO_2 NRs have high crystallinity (Fig. 1b). Compared with the synthesis of TiO_2 nanoparticles by Pan D et al. [23], we increased the TTIP concentration. According to the theory proposed by Peng's group [26], the higher initial precursor concentrations are preferable to the growth of one-dimensional nanocrystals. Hence, anisotropic TiO_2 NRs with small size are obtained in our synthesis. XRD patterns of TiO_2 NRs are presented in Fig. 2. The diffraction patterns of the samples indicate the presence of TiO_2 anatase with a typical anisotropic growth along the [101] direction [27]. The broadening peaks originate from small size of TiO_2 NRs. The TEM and XRD analyses indicate that anatase TiO_2 NRs are produced by the hydrothermal method.

3.2 Surface ligand exchange of TiO_2 NRs

Due to the hydrophobicity of oleic acid capped TiO_2 NRs (OLA-TiO_2 NRs), it is difficult to get a homogeneous paste for the doctor-blading process. It is essential to use a more hydrophilic ligand to exchange the oleophilic oleic acid on the surface of TiO_2 NRs. Here we use benzoic acid to exchange the oleic acid because it is a stronger acid than oleic acid with good solubility in ethanol.

Fig.3 shows the FTIR spectra in the region 4000-400 cm^{-1} of OLA-TiO_2 NRs and benzoic acid capped TiO_2 NRs (BA-TiO_2 NRs). As shown in Fig. 3, the broad band below 950 cm^{-1} in the FTIR spectra of all the TiO_2 NRs belongs to the characteristic vibrations of the inorganic Ti-O-Ti network [19]. For the FTIR spectrum of the OLA-TiO_2 NRs, the bands

at 2920 and 2852 cm^{-1} are assigned to the antisymmetric and symmetric C-H stretching vibrations of the $-CH_2-$ groups in the hydrocarbon moiety [28]. The shoulder at 2953 cm^{-1} results from the asymmetric stretching of the terminal $-CH_3$ group of the oleic acid molecule [28]. The intense bands at 1525 and 1432 cm^{-1} belong to the COO^- antisymmetric and symmetric stretching vibrations complexed with surface Ti centers, respectively [29]. Compared with the spectrum of OLA-TiO_2 NRs, the double bands at 1506 and 1407 cm^{-1} are observed clearly in the FTIR spectrum of BA-TiO_2 NRs, which can be attributed to the coordination between benzoic acid and TiO_2 [30]. The strong bands at 1384 cm^{-1} are connected to the symmetric stretching band of the COO^- group in the benzoic acid [31]. No vibrating bands of $-CH_2-$ and CH_3- groups can be observed, and that suggests oleic acid on the surface of TiO_2 NRs have been totally exchanged by the benzoic acid ligands.

3.3 Application in the DSSCs

The properties of the DSSCs are affected by the morphology of TiO_2 nanocrystals, the thickness and porosity of the TiO_2 photoanode films, and the counter electrode [32]. One-dimensional TiO_2 nanocrystals with direct charge transfer path are widely used in the photoanode of DSSCs. Ideally, all the one-dimentional TiO_2 NRs and nanowires should be aligned and connected to the FTO glass. However, the aligned TiO_2 NRs and nanowires are mostly with larger diameter (larger than 10 nm), which decreased the adsorption of dye [10]. From the earlier reports using small size TiO_2 NRs in the photoanode of DSSC, the NRs don't need to be aligned to get increased DSSC properties [16, 17]. In order to do the comparative study, all the DSSC devices based on the photoanodes of P25, OLA-TiO_2 NRs and BA-TiO_2 NRs were fabricated by doctor-blading methods under the same operating

conditions without blocking layer on the anode preventing shunt currents. And the TiO_2 density of per area for all the samples is 3.57 mg/cm^2.

Fig. 4 shows the SEM images of the OLA-TiO_2 NR and BA-TiO_2 NR films fabricated on FTO with the same thickness of around 12 μm. It can be seen that OLA-TiO_2 NR film has poor quality with the rough surface accompanied by some large aggregated particles. Because the OLA-TiO_2 NRs is hydrophobic, the OLA-TiO_2 NR paste is not homogeneous even with the addition of 30% PEO, which leads to the poor quality of doctor-bladed film on the FTO glass. After exchanging the oleic acid with benzoic acid, the quality of BA-TiO_2 NR film is increased significantly with the porous flat surface (Fig.4b).

Because of the large surface area of TiO_2 NRs with small size, an increase of dye adsorption in the photoanode of TiO_2 NR electrode is highly expected. Fig.5a shows the UV-vis absorption spectra of dye desorbed from the porous P25, OLA-TiO_2 NR and BA-TiO_2 NR film electrodes. It can be seen that the BA-TiO_2 NR-based photoanode film shows the increased dye adsorption by about 29 % compared with that of P25-based photoanode film. However, because of the poor quality of OLA-TiO_2 NR-based photoanode film, the dye adsorption of OLA-TiO_2 NR-based photoanode film is decreased by about 34% in relative to that of P25-based photoanode film. The measurements indicate that the application of TiO_2 NRs with small size in the photoanode films of DSSCs can combine the merits of large surface area and the direct charge transfer path.

The *J-V* characteristics of all the TiO_2 NR-based and P25-based DSSCs are shown on Fig.5b, and the photovoltaic data in terms of short circuit current density (*Jsc*), open circuit voltage (*Voc*), fill factor (*FF*), and power conversion efficiency (η) are listed at Table 1. The

BA-TiO_2 NR-based DSSC shows a *Voc* of 0.73 V, a *Jsc* of 14.30 mA cm^{-2}, a fill factor of 0.61, and an efficiency of 6.37 %, while the OLA-TiO_2 NR-based DSSC shows a *Voc* of 0.60 V, a *Jsc* of 5.25 mA cm^{-2}, a fill factor of 0.60, and an efficiency of 1.9 % under AM 1.5 simulated sunlight conditions. It clearly shows that the ligand exchange with benzoic acid significantly increases the photovoltaic properties, which is in good agreement with our SEM analysis and dye-adsorption analysis. The PCE of 6.37% for the BA-TiO_2 NR-based DSSC is much higher than that (4.89%) of former reported DSSC based on the oleic acid capped TiO_2 NR and TiO_2 nanoparticles electrodes [22]. Compared with the photovoltaic properties of P25-based DSSC, the DSSC based on BA-TiO_2 photoanode shows closer fill factor and open-circuit voltage, but higher short circuit current density. As a result, the power conversion efficiency was enhanced from 5.1% to 6.37% by using the BA-TiO_2 NR photoanode, which can be ascribed to the increased surface area and the better charge transfer of the one-dimentional TiO_2 NRs [17, 18].

In order to better understand the charge transfer and electron lifetime in the TiO_2 NR based DSSCs, electrochemical impedance spectroscopy (EIS) measurements were carried out at the frequency range of 1^{-1}~10^5 Hz at bias of 0.5 V under dark with the bias of 0.6 V. The Nyquist plots and the plot of imaginary parts of the impedance vs a function of frequency corresponding to the DSSCs based on the BA-TiO_2 NR photoanode and the P25 photoanode are shown in Fig. 6. In our EIS test, two arcs are detected for the DSSCs based on both BA-TiO_2 NRs and P25 based DSSCs. According to the reports by Hoshikawa et al. [33], they are assigned to impedances at TiO_2/dye/electrolyte interfaces, and the diffusion of the I^{3-}/I^- redox electrolyte. The charge transfer resistance of the platinized FTO counter electrode is not

detected because it is quite small with little change in comparison with the bare FTO anode. The semicircle diameter for BA-TiO_2 NR photoanode based DSSC increases evidently in comparison with that of P25 photoanode based DSSC, which indicates the increased charge transfer resistance at TiO_2/dye/electrolyte interfaces for the BA-TiO_2 NR based DSSC [34]. From Fig 6b, it can be deduced that the frequencies at which Im(Z) is a maximum for P25 photoanode based DSSC and BA-TiO_2 NR photoanode based DSSC are 3981 and 2326 Hz, respectively. It clearly indicates that the characteristic transport time at TiO_2/dye/electrolyte interface for BA-TiO_2 NR photoanode based DSSC is longer than that of P25 photoanode based DSSC. The longer charge transfer time at TiO_2/Dye/electrolyte for BA-TiO_2 NR-based DSSC effectively prevented the charge recombination of photogenerated electron with electrolyte, which leads to an increased efficiency of BA-TiO_2 NR photoanode based DSSC [35].

4. Conclusions

In summary, we reported the synthesis of anatase TiO_2 NRs with the diameter of 4-5 nm and the length of 30-50 nm by a simple two-phase hydrothermal method stabilized by oleic acid. The oleic acid ligand capped on the surface of TiO_2 NRs can be completely exchanged by benzoic acid ligand. The ligand exchange by benzoic acid can enhance the hydrophility of TiO_2 NRs for making uniform paste and improve the quality of TiO_2 NR based photoanode film on FTO glass. The corresponding DSSC based on BA-TiO_2 NR photoanode shows an enhanced PCE of 6.37% in comparison with that of 5.1% for the P25 based DSSC. The improved property of TiO_2 NR based DSSC is caused by the large surface area of TiO_2 NRs, the enhanced efficiency of charge transfer and collection in the TiO_2 NR photoanode, and the

decreased charge recombination at the TiO_2 NR photoanode/dye/electrode. It provides an alternative process to synthesize high-quality TiO_2 NRs on a large scale, which can be widely used in the application of solar cells and environmental engineering.

Acknowledgements

Authors would like to acknowledge the Clean Energy Research Programme under National Research Foundation of Singapore for their research grant (Grant No. NRF2007EWT-CERP01-0420) support for this work.

Reference

[1] O'Regan B, Grätzel M. A low-cost, high-efficiency solar cell based on dye sensitized colloidal TiO_2 films. Nature 1991; 353: 737-40.

[2] Nazeeruddin MK, Kay A, Rodicio I, Humphry-Baker R, Müller E, Liska P, Vlachopoulos N,Grätzel M. Conversion of light to electricity by cis-X2bis(2,2′-bipyridyl-4,4′-dicarboxylate) Ruthenium (II) charge-transfer sensitizers (X = Cl-, Br-, I-, CN-, and SCN-) on nanocrystalline TiO_2 electrodes. J. Am. Chem. Soc. 1993; 115; 6382-90.

[3] Nazeeruddin MK, Angelis FD, Fantacci S, Selloni A, Viscardi G, Liska P, Ito S, Takeru B, Grätzel M. Combined experimental and DFT-TDDFT computational study of photoelectrochemical cell ruthenium sensitizers. J. Am. Chem. Soc. 2005; 127: 16835- 47.

[4] Grätzel M. Dye-sensitized solar cells. J. Photoch. Photobio. C. 2003; 4: 145-53.

[5] Kopidakis N, Benkstein KD, Van De Lagemaat J, Frank AJ. Influence of the percolation network geometry on electron transport in dye-sensitized titanium dioxide solar cells. J. Phys. Chem. B 2003; 107: 7759-67.

[6] Solbrand A, Henningsson A, Sodergren S, Lindstrom H, Hagfeldt A, Lindquist SE. Charge transport properties in dye-sensitized nanostructured TiO_2 thin film electrodes studied by photoinduced current transients. J. Phys. Chem. B 1999; 103: 1078-83.

[7] Huynh WU, Dittmer JJ, Alivisatos AP. Hybrid nanorod-polymer solar cells. Science 2002; 295: 2425-7.

[8] Sun BQ, Marx E, Greenham NC. Photovoltaic devices using blends of branched CdSe nanoparticles and conjugated polymers. Nano. Lett. 2003; 3: 961-3.

[9] Liu J, Wang W, Yu H, Wu Z, Peng J, Cao Y. Surface ligand effects in MEH-PPV/TiO_2 hybrid solar cells. Sol. Energy Mater. Sol. Cells 2008; 92: 1403-9.

[10] Adachi M, Murata Y, Takao J, Jiu J, Sakamoto M, Wang F. Highly efficient dye-sensitized solar cells with a titania thin-film electrode composed of a network structure of single-crystal-like TiO_2 nanowires made by the "oriented attachment" mechanism. J. Am. Chem. Soc. 2004; 126: 14943-9.

[11] Jiu J, Isoda S, Wang F, Adachi M. Dye-sensitized solar cells based on anatase TiO_2 nanoparticle/nanowire composites. J. Phys. Chem. B 2006; 110: 15932-8.

[12] Song MY, Kim DK, Ihn KJ, Jo SM, Kim DY. New application of electrospun TiO_2 electrode to solid-state dye-sensitized solar cells. Synth. Metal. 2005; 153: 77-80.

[13] Tan B, Wu Y. Dye-sensitized solar cells based on a single-crystalline TiO_2 nanorod film. J. Phys. Chem. B 2006; 110: 2087-92.

[14] Song MY, Ahn YR, Jo SM, Kim DY, Ahn JP. TiO_2 single-crystalline nanorod electrode for quasi-solid-state dye-sensitized solar cells. Appl. Phys. Lett. 2005; 87: 1-3.

[15] Liu B, Aydil ES. Growth of oriented single-crystalline rutile TiO_2 nanorods on transparent conducting substrates for dye-sensitized solar cells. J. Am. Chem. Soc. 2009;

131: 3985-90.

[16] Kang SH, Choi SH, Kang MS, Kim JY, Kim HS, Hyeon T, Sung YE. Nanorod-based dye-sensitized solar cells with improved charge collection efficiency. Adv. Mater. 2008; 20: 54-8.

[17] Lee S, Cho IS, Lee JH, Kim DH, Kim DW, Kim JY, Shin H, Lee JK, Jung HS, Park NG, Kim K, Ko MJ, Hong KS. Two-step sol-gel method-based TiO_2 nanoparticles with uniform morphology and size for efficient photo-energy conversion devices. Chem. Mater. 2010; 22: 1958-65.

[18] Marco LD, Manca M, Giannuzzi R, Malara F, Melcarne G, Ciccarella G, Zama I, Cingolani R, Gigli G. Novel preparation method of TiO_2-nanorod-based photoelectrodes for dye-sensitized solar cells with improved light-harvesting efficiency. J. Phys. Chem. C 2010; 114: 4228-36.

[19] Cozzoli PD, Kornowski A, Weller H. Low-temperature synthesis of soluble and processable organic-capped anatase TiO_2 nanorods. J. Am. Chem. Soc. 2003; 125: 14539 -48.

[20] Zhang Z, Zhong X, Liu S, Li D, Han M. Aminolysis route to monodisperse titania nanorods with tunable aspect ratio. Angew.Chem. Int. Ed. 2005; 44: 3466-70.

[21] Joo J, Kwon SG, Yu T, Cho M, Lee J, Yoon J, Hyeon T. Large-scale synthesis of TiO_2 nanorods via nonhydrolytic sol-gel ester elimination reaction and their application to photocatalytic inactivation of E. coli. J. Phys. Chem. B 2005; 109: 15297-302.

[22] Saji VS, Pyo M. Dye sensitized solar cell of TiO_2 nanoparticle/nanorod composites prepared via low-temperature synthesis in oleic acid. Thin Solid Films 2010; 518:

6542-6.

[23] Pan D, Zhao N, Wang Q, Jiang S, Ji X, An L. Facile Synthesis and characterization of luminescent TiO_2 nanocrystals. Adv. Mater. 2005; 17: 1991-5.

[24] Li J, Tang S, Lu L, Zeng HC. Preparation of nanocomposites of metals, metal oxides, and carbon nanotubes via self-assembly. J. Am. Chem. Soc. 2007; 129: 9401-9.

[25] Wang ZS, Kawauchi H, Kashima T, Arakawa H. Significant influence of TiO_2 photoelectrode morphology on the energy conversion efficiency of N719 dye-sensitized solar cell. Coord. Chem. Rev. 2004; 248: 1381-9.

[26] Peng ZA, X. Peng. Nearly monodisperse and shape-controlled CdSe nanocrystals via alternative routes: nucleation and growth. J. Am. Chem. Soc. 2002; 124: 3343-53.

[27] Jun YW, Casula MF, Sim JH, Kim SY, Cheon J, Alivisatos AP. Surfactant-assisted elimination of a high energy facet as a means of controlling the shapes of TiO_2 nanocrystals. J. Am. Chem. Soc. 2003; 125: 15981-5.

[28] Thistlethwaite PJ, Hook MS. Diffuse reflectance Fourier Transform Infrared study of the adsorption of oleate/oleic acid onto titania. Langmuir 2000; 16: 4993-8.

[29] Nara M, Torii H, Tasumi M. Correlation between the vibrational frequencies of the carboxylate group and the types of its coordination to a metal ion: An *ab Initio* molecular orbital study. J. Phys. Chem. 1996; 100: 19812-7.

[30] Liao LF, Lien CF, Shieh DL, Chen FC, Lin JL. FTIR study of adsorption and photochemistry of amide on powdered TiO_2: comparison of benzamide with acetamide. Phys.Chem.Chem. Phys. 2002; 4: 4584-9.

[31] Wan C, He T, Gao X, Li J, Xin H**,** Liu FC. Relation between sers intensity and

electronic structures for a series of compounds $C_6H_5(CH_2)_n$ COOH (n = 0, 1, 2). J. Mol. Struc.1986; 140: 227-34.

[32] Hagfeldt A, Grätzel M. Molecular photovoltaics. Acc. Chem. Res. 2000; 33: 269-77.

[33] Hoshikawa T, Yamada M, Kikuchi T, Eguchi K. Impedance analysis of internal resistance affecting the photoelectrochemical performance of dye-sensitized solar cells. J. Electrochem. Soc. 2005; 152: E68- E73

[34] Wang Q, Moser JE, Grazel M. Electrochemical impedance spectroscopic analysis of dye-sensitized solar cells, J. Phys. Chem. B 2005; 109: 14945-53.

[35] Wang Q, Ito S,Gratzel M, Fabregat-Santiago F, Mora-Sero I, Bisquert J, Bessho T, Imai H. Characteristics of high efficiency dye-sensitized solar cells. J. Phys. Chem. B 2006; 110: 25210-21.

Figure captions and tables

Fig. 1. TEM image and HR TEM of oleic acid capped TiO_2 nanrods.

Fig. 2. X-ray diffraction patterns of oleic acid capped TiO_2 nanrods and P25.

Fig. 3. FTIR spectra of OLA-TiO_2 NRs and BA-TiO_2 NRs.

Fig. 4. SEM images for OLA-TiO_2 NR photoanode film and BA-TiO_2 NR photoanode Films

Fig. 5. (a) UV-vis absorption spectra of dye desorbed from OLA-TiO_2 NR photoanode film, BA-TiO_2 NR photoanode film and P25 photoanode film. (b) *J–V* characteristics of OLA-TiO_2 NR, BA-TiO_2 NR and P25 based dye-sensitized solar cells. The illumination intensity of 100 mW cm^{-2} with AM 1.5 and active area of 0.28 cm^2 were applied.

Fig. 6. Nyquist plots and the plot of imaginary parts of the impedance vs a function of frequency of DSSCs based on the BA-TiO_2 NR photoanode and P25 photoanode.

Table 1. Properties of dye-sensitized solar cells based on the OLA-TiO_2 NR, BA-TiO_2 NR and P25 TiO_2 photoanodes.

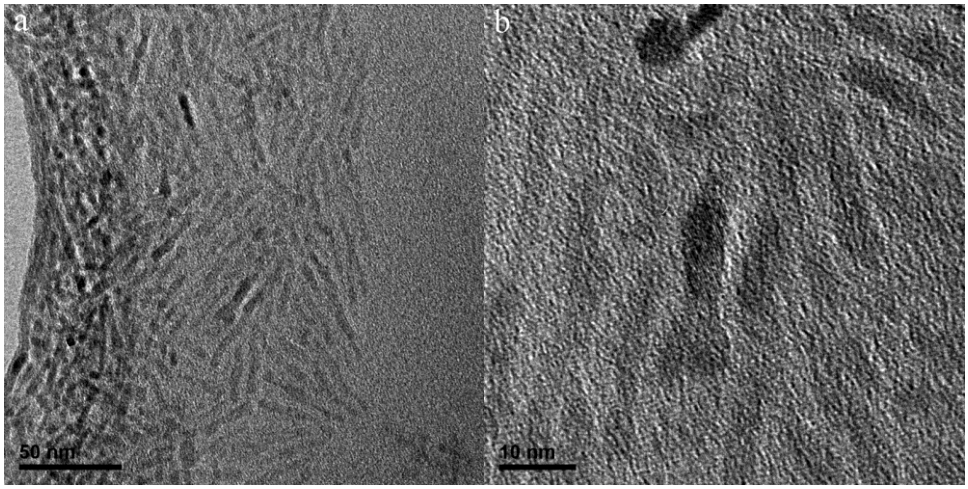

Fig. 1. TEM image and HR TEM of oleic acid capped TiO_2 nanrods.

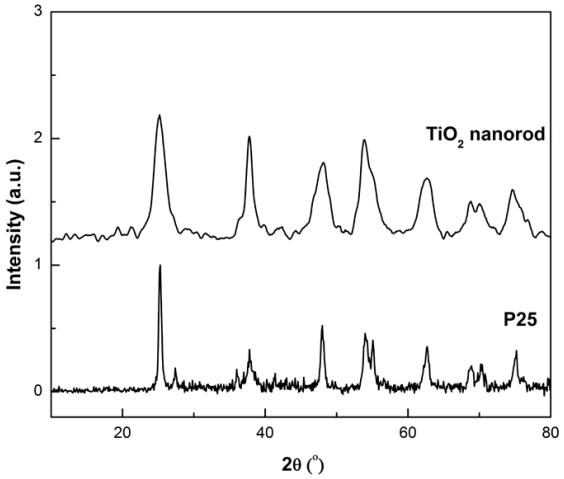

Fig. 2. X-ray diffraction patterns of oleic acid capped TiO_2 nanrods and P25.

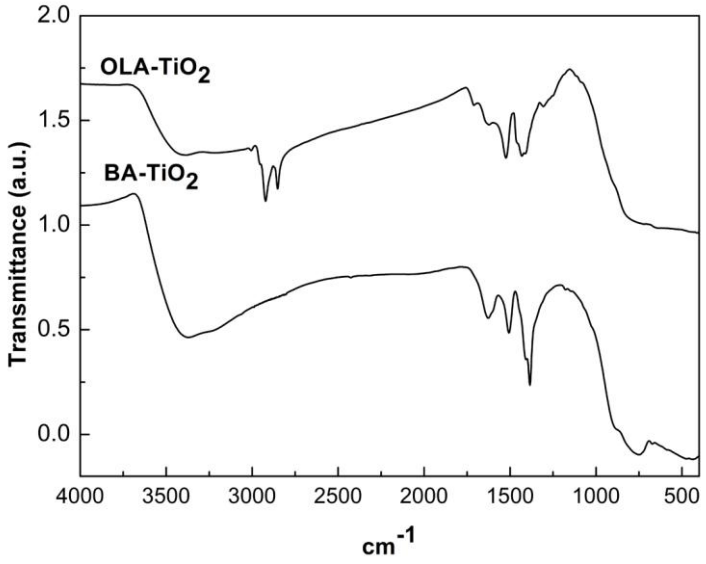

Fig. 3. FTIR spectra of OLA-TiO_2 NRs and BA-TiO_2 NRs.

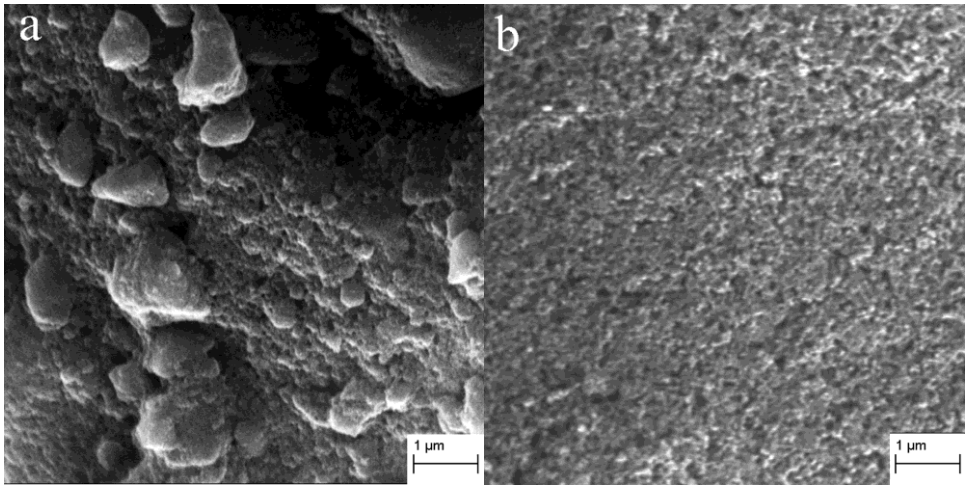

Fig. 4. SEM images for OLA-TiO_2 NR photoanode film（a） and BA-TiO_2 NR photoanode films (b).

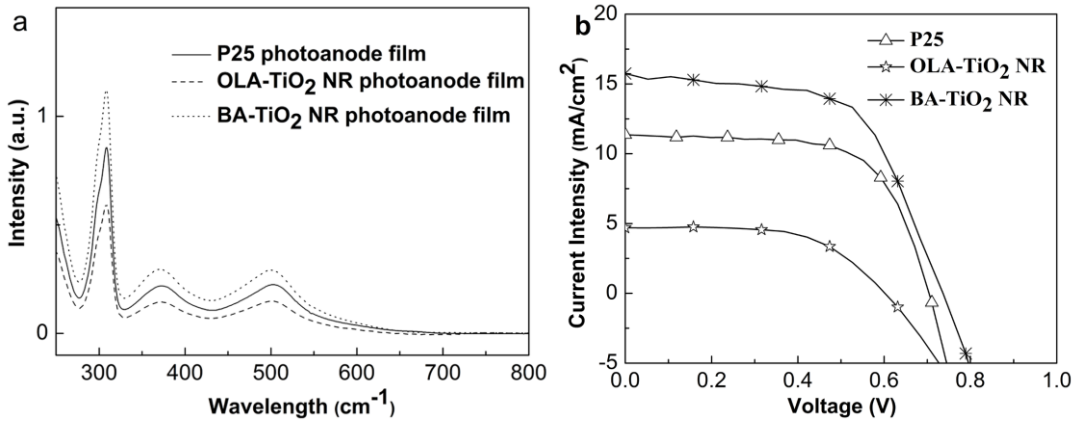

Fig. 5. (a) UV-vis absorption spectra of dye desorbed from OLA-TiO_2 NR photoanode film, BA-TiO_2 NR photoanode film and P25 photoanode film. (b) *J–V* characteristics of OLA-TiO_2 NR, BA-TiO_2 NR and P25 based dye-sensitized solar cells. The illumination intensity of 100 mW cm^{-2} with AM 1.5 and active area of 0.28 cm^2 were applied.

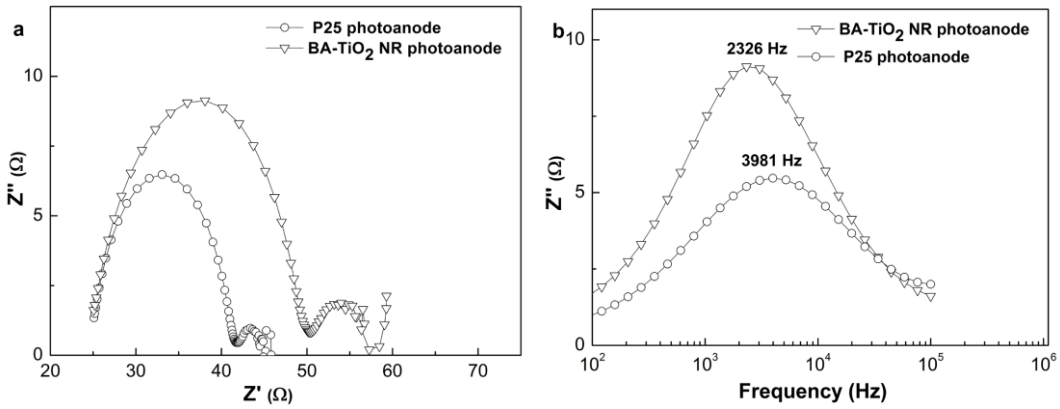

Fig. 6. Nyquist plots (a) and the plot of imaginary parts of the impedance vs a function of frequency (b) of DSSCs based on the BA-TiO_2 NR photoanode and P25 photoanode.

Table 1. Properties of dye-sensitized solar cells based on the OLA-TiO_2 NR, BA-TiO_2 NR and P25 TiO_2 photoanodes.

TiO_2	Thickness of TiO_2 electrode (μm)	J_{sc} (mA/cm^{-2})	V_{oc} (V)	FF (%)	η（%）
P25	12 μm	11.36	0.71	63.4	5.1
OLA-TiO_2 NRs	12 μm	5.25	0.60	60.1	1.9
BA-TiO_2 NRs	12 μm	14.30	0.73	60.5	6.37